ASCE

Levee Fragility Behavior under Projected Future Flooding in a Warming Climate

Farshid Vahedifard, M.ASCE[1]; Firas H. Jasim, S.M.ASCE[2]; Fred T. Tracy[3]; Masood Abdollahi, S.M.ASCE[4]; Aneseh Alborzi[5]; and Amir AghaKouchak, M.ASCE[6]

Abstract: Adaptation to climate change requires careful evaluation of infrastructure performance under future climatic extremes. This study demonstrates how a multidisciplinary approach integrating geotechnical engineering, hydrology, and climate science can be employed to quantify site-specific impacts of climate change on geotechnical infrastructure. Specifically, this paper quantifies the effects of changes in future streamflow on the performance of an earthen levee in Sacramento, California, considering multiple modes of failure. The streamflows for historical (1950–2000) and projected (2049–2099) scenarios with different recurrence intervals were derived from routed hydrological simulations driven by bias-corrected global climate models. The historical and future flood levels were then applied in a set of transient coupled finite-element seepage and limit equilibrium slope stability analyses to simulate the levee subjected to extreme streamflow. Variability in hydraulic and mechanical properties of soils was addressed using a Monte Carlo sampling method to evaluate and compare the probability of failure of the levee under different historical and future climate scenarios. Three individual modes (underseepage, uplift, and slope stability) along with lower and upper bounds for the combined mode of failure were examined. The results showed that incorporating future floods into levee failure analysis led to considerable reductions in the mean factor of safety and increases in the levee's probability of failure, suggesting that risk assessment based on historical records can significantly underestimate the levee's failure probability in a warming climate. Despite inherent uncertainties in future projections and substantial variability across climate models, evaluating infrastructure against projected extremes offers insights into their likely performance for the future. **DOI: 10.1061/(ASCE)GT.1943-5606.0002399.**

Author keywords: Climate change; Adaptation; Levees; Probability of failure; Streamflow; Numerical modeling; Process-informed nonstationary extreme value analysis (ProNEVA).

Introduction

Historical observations show considerable changes in type, severity, frequency, and duration of extreme precipitation and flood events across the world (Groisman et al. 2004; USGCRP 2009; IPCC 2013). For instance, ground-based observations show a 9% increase in heavy precipitations from 1958 to 2012 (USGCRP 2009). Additionally, partly attributed to anthropogenic activities, climate models project increases in the intensity and frequency of future extreme precipitation and flooding (e.g., Florsheim and Mount 2003; Ragno et al. 2019). In the United States, the impact of the annual flood-related damage to infrastructure has increased significantly since 1934 (Pielke et al. 2002), attributed to both increased exposure and changes in the frequency and severity of extremes. A warming climate is expected to increase the water-holding capacity of the atmosphere, which can intensify precipitation extremes and flood risk (Trenberth 2001; Papalexiou and Montanari 2019; Chen and Hossain 2019).

Adaptation to climate change requires evaluations of infrastructure performance for extreme events such as flooding for different emission scenarios (e.g., Vardon 2015; CACC 2018; Forzieri et al. 2018; Hagenlocher et al. 2018; Reidmiller et al. 2017; Vahedifard et al. 2018; Fletcher et al. 2019). Changes in statistics of extreme precipitation and floods in a changing climate can significantly affect the stability of natural and man-made earthen structures, including levees (e.g., Robinson and Vahedifard 2016; Jasim et al. 2017; Robinson et al. 2017; Vahedifard et al. 2017; CACC 2018; FEMA 2018). The severity of damage to levees depends on the structural integrity of the levee as well as the intensity, duration, and frequency characteristics of extreme climatic events such as rainfalls, floods, and even droughts (e.g., Vahedifard et al. 2016). The structural integrity of levees subjected to extreme events and loading conditions can be threatened by one or more modes of failure, such as slope stability, underseepage, uplift, through seepage, and overtopping.

Over the past few decades, several methods have been employed for risk and reliability analyses of levees under various loading conditions (e.g., Wood 1977; Wolff 2008; Wu et al. 2011; Ludy and Kondolf 2012; Jongejan and Calle 2013; Zhang et al. 2013;

[1]Civil and Environmental Engineering Advisory Board Endowed Professor and Associate Professor, Dept. of Civil and Environmental Engineering, Mississippi State Univ., Mississippi State, MS 39762 (corresponding author). ORCID: https://orcid.org/0000-0001-8883-4533. Email: farshid@cee.msstate.edu

[2]Lecturer, Dept. of Civil Engineering, Tikrit Univ., Tikrit 34001, Iraq; formerly, Ph.D. Student, Dept. of Civil and Environmental Engineering, Mississippi State Univ., Mississippi State, MS 39762. Email: firasarab@tu.edu.iq

[3]Research Computer Scientist Emeritus, Information Technology Laboratory, Engineer Research and Development Center, US Army Corps of Engineers, Vicksburg, MS 39180. Email: Fred.T.Tracy@usace.army.mil

[4]Ph.D. Student, Dept. of Civil and Environmental Engineering, Mississippi State Univ., Mississippi State, MS 39762. ORCID: https://orcid.org/0000-0002-5273-2073. Email: ma1882@msstate.edu

[5]Ph.D. Student, Dept. of Civil and Environmental Engineering, Univ. of California, Irvine, CA 92697. ORCID: https://orcid.org/0000-0003-2233-889X. Email: aalborzi@uci.edu

[6]Professor, Dept. of Civil and Environmental Engineering, Univ. of California, Irvine, CA 92697. Email: amir.a@uci.edu

Note. This manuscript was submitted on July 24, 2019; approved on July 8, 2020; published online on September 30, 2020. Discussion period open until February 28, 2021; separate discussions must be submitted for individual papers. This paper is part of the ***Journal of Geotechnical and Geoenvironmental Engineering***, © ASCE, ISSN 1090-0241.

Hui et al. 2016; Roe et al. 2016; Bessette et al. 2017; Jasim et al. 2017; Schultz et al. 2018; Lanzafame and Sitar 2019; Rahimi et al. 2019; USBR 2019; Zimmaro et al. 2019). These methods include expert judgment, empirical, analytical, and hybrid methods, depending upon the source of knowledge used to assess the probability of failure, or the probability of unsatisfactory performance, versus the range of levee loads (e.g., Schultz et al. 2010). The probability of failure-load relationship is commonly referred to as a fragility curve (or system response curve), a useful tool for levee risk analysis (e.g., Schultz et al. 2010; USBR 2019). Among others, the analytical method, which is based on quantitative models of load and resistance, is shown to be best suited for robust risk analysis (e.g., Schultz et al. 2018; Lanzafame and Sitar 2019; USBR 2019; Zimmaro et al. 2019). In this approach, the levee's probability of failure is estimated by considering the uncertainly in one or more variables (e.g., soil types, soil properties, levee geometry and dimensions, and water level) that affect load or resistance.

This study demonstrates how hydrology and climate science findings can be employed to quantify site-specific impacts of climate change on earthen levees. We quantified the effects of extreme streamflow in a changing climate on the performance of an earthen levee considering multiple failure modes. Historical (1950–2000) and future (2049–2099) streamflow simulations were derived from bias-corrected global climate models and routed hydrologic simulations, developed for the 4th California Climate Change Assessment (Pierce et al. 2015, 2018). Floods with different climatic extreme recurrence intervals were then employed as hydraulic loads into a set of transient coupled finite-element seepage and limit equilibrium slope stability analyses to simulate the levee subjected to extreme streamflow. Considering the variability in the hydraulic and mechanical properties of soils, the numerical modeling framework was used along with the Monte Carlo method to evaluate the probability of failure of the levee against individual and combined modes of failure, including underseepage, uplift, and slope stability.

Study Area

Over 21,000 km of levees protect land and infrastructure from floods in California (CDWR 2011). However, most of these levees work under relatively marginal conditions (CDWR 2011), which is comparable to the overall grade of the nation's levee systems (ASCE 2017). According to a 155-year observational data record from a California river system, structural failures have occurred in more than 25% of the earthen levees during the last century (Florsheim and Dettinger 2007). Rapidly growing urbanization, socioeconomic importance of the region, marginal conditions, and continuous exposure to a variety of natural hazards and climate extremes (e.g., earthquakes, land subsidence, droughts, floods, and wildfires) have stimulated several studies over the past few decades to assess the vulnerability and risk associated with California's levee systems (e.g., Deverel and Leighton 2010; Brooks et al. 2012; LAO 2015; Vahedifard et al. 2015, 2016; Hui et al. 2016; Roe et al. 2016; Deverel et al. 2016; Robinson and Vahedifard 2016; Jasim et al. 2017; Hui et al. 2018; Lanzafame and Sitar 2019; Zimmaro et al. 2019).

For modeling, we studied the Elkhorn Levee, an earthen levee in a high-risk flooding zone (Reclamation District No. 1000) in Sacramento, California (Fig. 1). Levee systems throughout the Northern California Central Valley are often urban and protect densely populated areas from flooding (CDWR 2011). Many of these levees are loaded only during flooding or high water. In contrast, the levees throughout most of the Delta downstream of Sacramento are mainly nonurban, protecting land that is at or below sea level, and continuously hold back water.

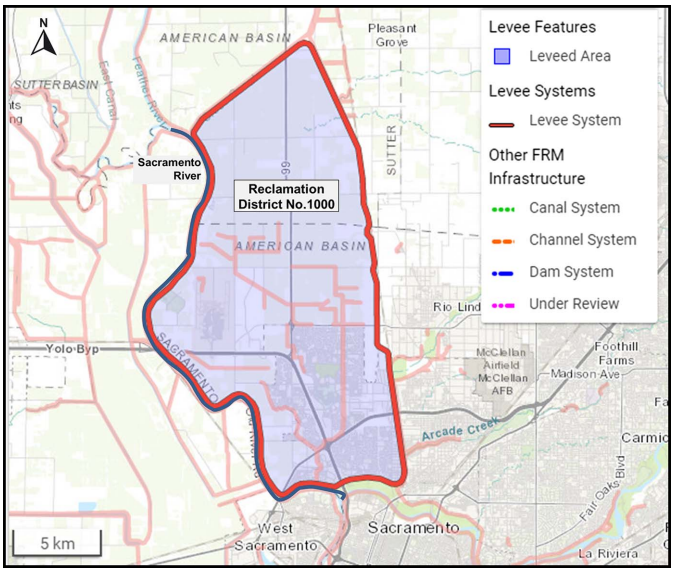

Fig. 1. Leveed area in Reclamation District No. 1000, Sacramento, California. (Reprinted from NLD 2020.)

Streamflow Loading in a Changing Climate

Current practices for design and risk assessments of infrastructure systems commonly rely on observed historical extremes, such as rainfall and flood records, assuming the statistics of extremes do not change significantly over time (Cheng et al. 2014; Salas and Obeysekera 2014). Here, we incorporated future flood projections into the risk analysis of the Elkhorn Levee. Unlike common statistical proxies to estimate future river discharge (e.g., Kundzewicz et al. 2014; Wobus et al. 2014; Hui et al. 2018), we employed projected future streamflow derived from global climate models and hydrologic simulations. The Elkhorn Levee is adjacent to Camp Far West, one of the 59 locations across Northern California where daily streamflow projections (1950–2099) were developed, bias corrected, and routed as part of the California Fourth Climate Change Assessment project (Pierce et al. 2014, 2015, 2018). The variable infiltration capacity (VIC) hydrological model (Lohmann et al. 1996, 1998), which simulates surface and subsurface processes, was forced with downscaled global climate model (GCM) simulations to route daily streamflow. The bias-corrected inputs to the hydrologic model (VIC) were based on ten GCMs from the Fifth Coupled Model Intercomparing Project (CMIP5) and two representative concentration pathways (RCPs): RCP4.5 and RCP8.5.

For flood risk assessment in the Elkhorn Levee, we employed RCP8.5 data and the most extreme projected streamflow scenario from the CanESM2 model, one of four representative climate models for California. Pierce et al. (2018) and Thorne et al. (2018) provided more information on representative models for the state of California. We ran flood frequency analysis using process-informed nonstationary extreme value analysis (ProNEVA, Ragno et al. 2019; Cheng et al. 2014) to identify flood magnitudes for different recurrence intervals (White 1976; Groves et al. 2006). We used daily annual flow maxima for flood frequency analysis, as it is a key design variable and the most commonly used variable for flood risk assessment when instantaneous observations are unavailable (e.g., England et al. 2019). The streamflow design load was represented by the

Table 1. Streamflow and corresponding flood level for different recurrence intervals using historical and projected future data

Recurrence interval (years)	Levee loading	Historical (1950–2000)	Future (2049–2099)
10	Streamflow (m^3/s)	613.86	1,073.07
	Flood level (m)	18.33	20.46
25	Streamflow (m^3/s)	858.83	1,308.43
	Flood level (m)	19.54	21.38
50	Streamflow (m^3/s)	1,095.59	1,478.50
	Flood level (m)	20.56	21.90

flood water level behind the levee. Applying the rating curve concept (i.e., river stage and discharge relationship at the gauging station), we estimated the flood water level corresponding to the design streamflow for different recurrence intervals (e.g., 25- and 50-year flood events).

Table 1 shows the streamflow and flood level for different recurrence intervals using the historical (1950–2000) and projected future (2049–2099, RCP 8.5) simulations. The future flood levels from the CanESM2 model, for all recurrence intervals, show higher peak water levels compared to baseline (1950–2000) flood levels simulations, implying higher flood risk in the future, consistent with the findings of Mallakpour et al. (2018). The future flood simulations had a 1.34-m higher flood level than the baseline period for the 50-year event, a 6.5% increase.

Probability of Failure Considering Different Modes of Failure

In this study, the probability of unsatisfactory performance, hereafter referred to as the probability of failure, was calculated by treating the soils' hydromechanical properties as random variables. The performance function, $G(\boldsymbol{X})$, can be defined as

$$G(\boldsymbol{X}) = G(R,S) = \frac{G_R(\boldsymbol{X})}{G_S(\boldsymbol{X})} \tag{1}$$

where $\boldsymbol{X}$ = vector of random variables; $S = G_s(\boldsymbol{X})$ is the load imposed on the levee; and $R = G_R(\boldsymbol{X})$ is the capacity of levee to resist the load. In this equation, $G(R,S)$ represents the factor of safety, which is the ratio of the capacity to resist a demand (i.e., load) placed on the levee. When $G(\boldsymbol{X})$ is less than the predefined performance criteria [$G_{\text{design}}(\boldsymbol{X})$], the performance of the levee is considered unsatisfactory. The probability of failure for the ith mode of failure ($P_{f,i}$) is determined by integrating the multivariate density function, $f_X(\boldsymbol{X})$, for the n-dimensional vector of random variables over the unsatisfactory performance domain (e.g., Schultz et al. 2018)

$$P_{f,i} = P[G(\boldsymbol{X}) < 1] = \int \cdots \int_{G(\boldsymbol{X})<\mathrm{G}_{\text{design}}(X)} f_X(\boldsymbol{X})d\boldsymbol{X} \tag{2}$$

The historical and future flood levels were applied in a set of coupled transient finite-element seepage and limit equilibrium slope stability analyses to simulate the levee subjected to extreme streamflow. The Monte Carlo method with 6,000 realizations of soil properties (treated as random variables) was used to estimate the probability of failure for each mode at each water level. The input data sets needed for the Monte Carlo simulation were from sampling the probability distributions of uncertain mechanical and hydraulic properties of each soil type [based on its unified soil classification system (USCS) classification] in the levee embankment and foundation. A total of 11 random variables (including sampled and derived variables) for each soil type were considered, covering mechanical and hydraulic properties of the soil layers in saturated and unsaturated conditions (see the section "Soil Properties and Random Variables" for more details). Each realization was examined to see if the levee met the performance criteria defined for underseepage, uplift, and slope stability. The probability of failure at selected times during the simulation was calculated as the fraction of 6,000 realizations that failed to satisfy the performance criteria for that failure mode. The following performance functions were used for different modes of failure:

$$G(R,S)_{un} < \frac{0.33 i_{cv}}{i_v} \tag{3}$$

$$G(R,S)_{up} < \frac{0.667 u_t}{u_u} \tag{4}$$

$$G(R,S)_{sl} < 0.909\left(\frac{\tau}{\tau_f}\right)_{\min} \tag{5}$$

where $G(R,S)_{un}$, $G(R,S)_{up}$, and $G(R,S)_{sl}$ = performance functions for underseepage, uplift, and slope stability modes of failure, respectively; i_{cu} = critical vertical exit gradient at the landside toe of the levee; i_v = vertical exit gradient at the landside toe of the levee; u_t = pressure applied by the weight of the saturated soil at the toe beneath the confining layer of the levee; u_u = uplift pressure at the same location; τ = shear stress; and τ_f = shear strength of the soil along the most critical failure surface sought in the limit equilibrium slope stability analysis of the landside levee slope. The aforementioned performance functions embody the following factors of safety: 3 for underseepage, 1.5 for uplift, and 1.1 for slope stability. These values were selected within the range of recommended values by guidelines for design and risk analysis of earthen levees (e.g., USACE 2000; USBR 2019).

After estimating the probability of failure for each mode, the combined probability of failure can be calculated. As discussed by Lendering et al. (2018), the upper and lower bounds of the combined probability of failure can be determined by assuming mutual exclusivity (upper bound) or complete dependence (lower bound) between n modes of failure as follows:

$$\max(P_{f,i}) \le P_{f,t} \le \sum_{i=1}^{n} P_{f,i} = 1 - \prod_{i=1}^{n}(1 - P_{f,i}) \tag{6}$$

where $P_{f,t}$ = combined (aggregate) probability of failure. Most previous studies (e.g., Wolff 2008; Rice and Polanco 2012; Jongejan et al. 2013; Bogárdi and Balogh 2014; Schultz et al. 2018; Lendering et al. 2018) determine the combined probability of failure of earthen levees by assuming independence among failure modes. However, different failure modes can be somewhat dependent, because they share common triggering and resisting factors. To properly represent the range of possible $P_{f,t}$ values, we considered and presented both lower and upper bounds in this study. Other possible uncertainties not considered in this study include uncertainties in the response threshold, model error, and flood scenarios. The latter itself includes uncertainties from intermodel variability when multiple models are used, and uncertainties from future RCPs.

Numerical Modeling

Probabilistic numerical simulations were performed using two codes, SEEP2D-COUPLED-HPC and SLOPE2D-HPC (Tracy et al. 2020).

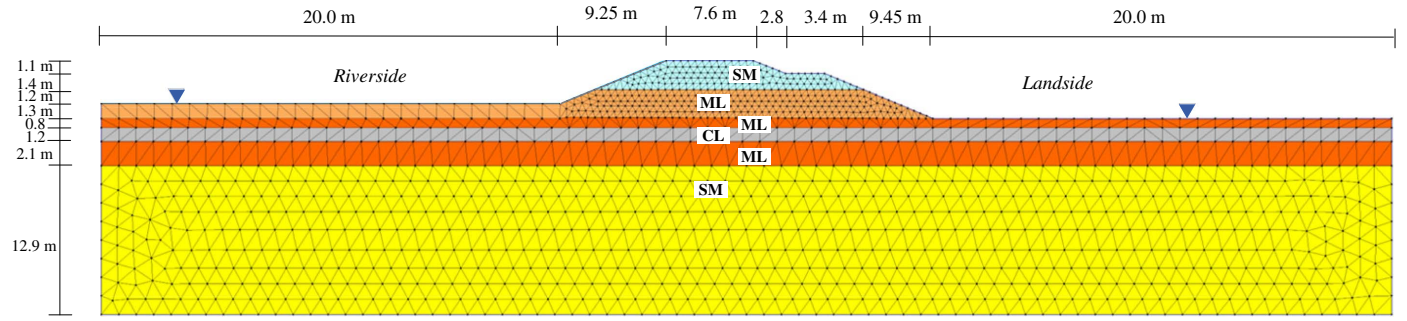

Fig. 2. Geometry of Elkhorn Levee used in numerical modeling.

The former is a two-dimensional coupled transient finite-element seepage/structural plane strain program designed to run on the US Army Engineer Research and Development Center (ERDC)'s high-performance computing facticity, whereas the latter is a limit equilibrium slope stability code that uses the simplified Bishop method. The pore-water pressures obtained from the coupled finite-element seepage are incorporated into the limit equilibrium slope stability analysis. Geometry and soil types were assumed to be known. Parameters describing the hydraulic and mechanical properties of soils were treated as uncertain variables, while the geometry of the two-dimensional levee section was held constant. It is noted that a similar probabilistic modeling framework is currently being used by the USACE (Schultz et al. 2018; Tracy et al. 2020) to examine the fragility behavior of an extensive array of USACE portfolio of levees throughout the nation. Employing this method allows performing site-specific probabilistic analysis for levees with limited in situ data (such as geometry and soil type) while accounting for the uncertainly of soil parameters. This feature makes the method broadly applicable to the nation's portfolio of levees. Further, the probabilistic method is objective, rigorous, and quantitative (Schultz et al. 2018; Tracy et al. 2020).

Theory of Coupled Seepage Analysis in Variably Saturated Soils

Transient flow under an elevating water level can be described using Laplace's equation as follows:

$$\frac{\partial}{\partial x}\left(k_x\frac{\partial \emptyset}{\partial x}\right)+\frac{\partial}{\partial y}\left(k_y\frac{\partial \emptyset}{\partial y}\right)=m_v\frac{\partial \emptyset}{\partial t} \tag{7}$$

where x = horizontal direction; y = vertical direction; k_x and k_y = hydraulic conductivities in the x- and y-directions; $\emptyset$ = total head; m_v = coefficient of soil volume compressibility; and t = time. The coupled governing equation for conservation of flow can be written as (Tracy et al. 2020)

$$\frac{\partial}{\partial x}\left(k_x\frac{\partial \emptyset}{\partial x}\right)+\frac{\partial}{\partial y}\left(k_y\frac{\partial \emptyset}{\partial y}\right)=\frac{\partial}{\partial t}\left(\frac{\partial u}{\partial x}+\frac{\partial v}{\partial y}\right) \tag{8}$$

where u and v = displacements in the x- and y-directions, respectively. The derivation of displacement with respect to the horizontal and vertical directions can be determined using the conservation of forces inside a finite element:

$$\begin{Bmatrix}\sigma_{xx}\\ \sigma_{yy}\\ \tau_{xy}\end{Bmatrix}+\gamma_w(\emptyset-y)\begin{Bmatrix}1\\1\\0\end{Bmatrix}=[\mathbf{C}]\begin{Bmatrix}\frac{\partial u}{\partial x}\\ \frac{\partial v}{\partial y}\\ \frac{\partial v}{\partial x}+\frac{\partial u}{\partial y}\end{Bmatrix} \tag{9}$$

$$[\mathbf{C}]=\frac{E}{(1+\theta)(1-2\theta)}\begin{pmatrix}1-\mu & \mu & 0\\ \mu & 1-\mu & 0\\ 0 & 0 & \frac{1-2\mu}{2}\end{pmatrix} \tag{10}$$

where σ_{xx} = normal stress in the x-direction; σ_{yy} = normal stress in the y-direction; τ_{xy} = shearing stress; E = Young's modulus; and μ = Poisson's ratio.

For unsaturated soils, the model proposed by Fredlund and Xing (1994) was used to represent the soil-water retention curve (SWRC) as follows:

$$\theta(\psi)=C(\psi)\frac{\theta_s}{[\ln(e+(\frac{\psi}{a})^b)]^c} \tag{11}$$

where $\theta(\psi)$ = volumetric water content at matric suction (ψ); θ_s = saturated volumetric water content; ψ = matric suction; a, b, and c = fitting parameters; and $C(\psi)$ is defined as

$$C(\psi)=1-\frac{\ln\left(1+\frac{\psi}{C_r}\right)}{\ln\left(1+\frac{10^6}{C_r}\right)} \tag{12}$$

where C_r = constant related to matric suction at the residual water content. For the hydraulic conductivity function (HCF), the Fredlund et al. (1994) model was used as

$$k(\psi)=\frac{\int_{\ln\psi}^{10^6}\frac{\theta(e^z)-\theta(\psi)}{e^z}\theta'(e^z)d\psi}{\int_{\ln\psi}^{10^6}\frac{\theta(e^z)-\theta_0}{e^z}\theta'(e^z)d\psi}k_s \tag{13}$$

where z = dummy variable of integration representing $\ln\psi$; ε_a = small positive number; θ' = derivative of Eq. (11) with respect to ψ; and k_s = saturated hydraulic conductivity.

Model Geometry

Fig. 2 shows the cross section of the Elkhorn Levee numerically modeled to evaluate and compare the impacts of historical and projected future floods. The model consisted of a five-layer soil system. The levee's body is 3.7 m of silty sand (SM) over a deep foundation, consisting of a thin layer of sandy clay (CL) with low hydraulic

conductivity. Under the CL layer is a 2.1-m-thick layer of ML, and below that the soil is mostly silty sand (SM). The geometry was adopted and modified from that reported in Brizendine (1997) and Khalilzad et al. (2014).

Soil Properties and Random Variables

Three soil types (SM, ML, and CL) were used in the model, and for each soil type, a total of 11 random variables (including three sampled and eight derived random variables) and two deterministic properties were considered as input covering both the mechanical and hydraulic properties of soil layers under saturated and unsaturated conditions. Sampling from the probability distributions representing the uncertain mechanical and hydraulic properties of each soil type was performed to obtain data sets for the Monte Carlo simulation. Probability distributions were defined for (1) vertical saturated hydraulic conductivity, (2) anisotropy ratio with respect to hydraulic conductivity, (3) liquid limit, (4) plasticity index, (5) effective friction angle of coarse-grained soils, (6) porosity, and (7) percent fines. Three sampled variables out of the aforementioned seven variables were used directly as random variables into the seepage and slope stability analyses: vertical saturated hydraulic conductivity, effective friction angle of coarse-grained soils, and porosity. The sampled variables were assumed to be uncorrelated. Input values for the additional eight soil properties required to perform the seepage and slope stability simulations were derived from the aforementioned seven sampled random variables. Derived random variables include (1) horizontal saturated hydraulic conductivity, (2) saturated unit weight, (3) partially saturated unit weight, (4) undrained shear strength for foundation fine-grained soils, (5) SWRC parameter a, (6) SWRC parameter b, (7) SWRC parameter c, and (8) SWRC parameter C_r. Further details about these soil properties are provided in the following. It is noted that the soil properties and random variables are mostly adopted from Schultz et al. (2018) and Tracy et al. (2020).

Sampled Variables

- Vertical saturated hydraulic conductivity (k_v): The uncertainty in hydraulic conductivities is commonly shown using lognormal probability distribution (Baecher and Christian 2003). The parameters of a lognormal distribution of k_v for each soil class in the levee or foundation are reported in Table 2. The mean of the distribution was obtained by taking the midpoint between the log-transformed minimum and maximum. The standard deviation was obtained by assuming a coefficient of variation equal to 0.9, which produced extreme values that approximate these minimums and maximums.
- Anisotropy ratio (r): The anisotropy ratio, r, is the ratio of the vertical to the horizontal hydraulic conductivity ($r = k_v/k_h$). The variable is distributed lognormally. A mean of one was used for the sandy soils (SM), a mean of 0.5 was used for silty soils (ML), and a mean of 0.25 was used for clayey soils (CL). A coefficient of variation equal to 0.4 is reported for clay soils in USACE (1999). Silt and sand show less variability in r than clay soils. Thus, variation coefficients of 0.2 and 0.075 were considered for silt and sand, respectively. In this study, the same values of the anisotropy ratio were used for foundation and embankment soils of the same USCS class.
- Liquid limit (LL) and plasticity index (PI): Correlated values of LL and PI were obtained by sampling each from uniform random fields with upper and lower bounds as indicated in the plasticity chart (Fig. 3). Combinations of values between the U-line and the A-line were then randomly selected. The correlated random samples of LL and PI are shown in Fig. 3.
- Effective friction angle for coarse-grained soils (ϕ'): The effective friction angle was used to calculate the long-term strength of soil. For the SM layer in the foundation, values of ϕ' were sampled from symmetrical triangular distributions with minimum and maximum values reported by Holtz et al. (2011). For silty sand, SM: min = 29°, max = 37°.
- Porosity (n): Ranges of porosity were obtained from Holtz et al. (2011) and are as follows for different soil types: SM: min = 0.36, max = 0.45; ML: min = 0.40, max = 0.50; CL: min = 0.40, max = 0.52. A symmetric triangular distribution was assumed for porosity.
- Percent fines (w): Percent fines is the fraction of material by weight that is less than 0.075 mm in diameter. For the soil layer classified as SM, a uniform distribution with a lower bound of 0.12 and an upper bound of 0.4999 was used. For the soil layers classified as ML and CL, a uniform distribution with a lower bound of 0.5 and an upper bound of 0.65 was used.

Derived Variables

- Horizontal saturated hydraulic conductivity (k_H): Values of K_H were derived by multiplying the vertical saturated hydraulic conductivity (K_V) by the anisotropy ratio (r). Deriving K_H from K_V ensured that the two values were correlated. Soils with higher values of K_H also tend to have higher values of K_V.
- Saturated and partially saturated unit weight ($\gamma_{\text{sat}}, \gamma_p$): The saturated unit weight, γ_{Sat}, was calculated from void ratio $\gamma_{\text{Sat}} = (G + S_r \cdot e) \cdot \gamma_w \cdot (1 + e)^{-1}$, where G is the specific gravity of soil, $G = 2.68$; γ_w is the unit weight of water, $\gamma_w = 9.81\ \text{kN/m}^3$; e is the void ratio where $e = n/(1 - n)$; and S_r is the degree of saturation. For saturated soils below the phreatic surface, $S_r = 1$. For partially saturated soils above the phreatic

Table 2. Minimum and maximum values for k_v (m/s)

USCS	Horizontal hydraulic conductivity, k_v (m/s)			
	Minimum	Maximum	Mean	Standard deviation
SM	5.00×10^{-8}	5.00×10^{-6}	6.37×10^{-7}	6.05×10^{-7}
ML	5.00×10^{-9}	5.00×10^{-7}	6.37×10^{-8}	6.05×10^{-8}
CL	5.00×10^{-10}	5.00×10^{-8}	6.37×10^{-9}	6.05×10^{-9}

Source: Data from Holtz et al. (2011).

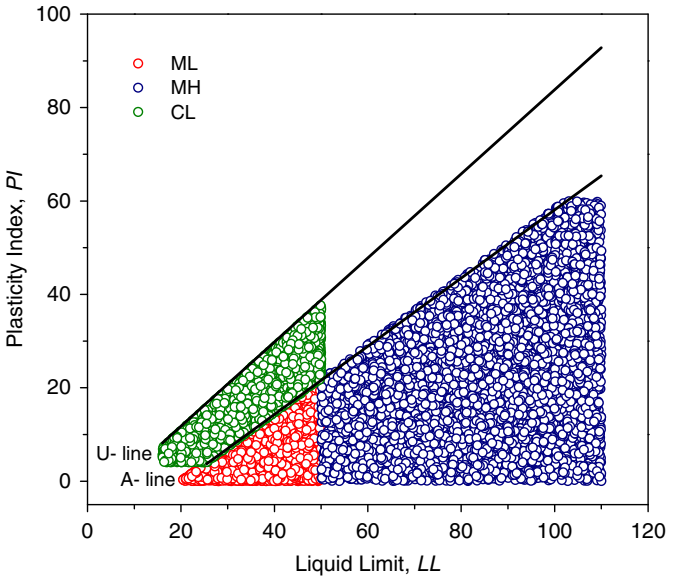

Fig. 3. Correlated random samples of LL and PI used in simulation. (Data from Schultz et al. 2018.)

surface, S_r was defined as a uniform random variable between 0.5 and 0.95.

- Undrained shear strength (S_u): For silts and clays in foundations, undrained shear strength S_u was defined as a function of the strength ratio (SR). SR is the ratio of the shear strength to the effective overburden pressure (σ_v'). Values of SR were obtained by sampling from asymmetrical triangular distributions in which its three parameters were calculated from PI using the correlations developed by Mayne (2012):

$$S_u = SR \cdot \sigma_v' \tag{14}$$

$$SR_{\min} = 0.05 + 0.0019PI \tag{15}$$

$$SR_{\max} = 0.35 + 0.0002PI \tag{16}$$

$$SR_{\mathrm{mod}} = 0.198 + 0.001PI \tag{17}$$

where $SR_{\min}$, $SR_{\max}$, and SR_{mod} = minimum, maximum, and mode of the distribution.

- SWRC and HCF parameters (a, b, c, and C_r): The SWRC and HCF parameters were sampled from symmetrical triangular distributions. The parameters of the SWRC and HCF models were correlated with the wPI parameter as follows (Witczak et al. 2000):

$$a = 0.00364(wPI)^{3.35} + 4(wPI) + 11 \tag{18}$$

$$\frac{b}{c} = -2.313(wPI)^{0.14} + 5 \tag{19}$$

$$c = 0.0514(wPI)^{0.465} + 0.5 \tag{20}$$

$$\frac{C_r}{a} = 32.44e^{0.0186(wPI)} \tag{21}$$

$$wPI = \text{percent fines} \times PI \tag{22}$$

Deterministic Soil Properties

- Modulus of elasticity (E): The modulus of elasticity, E, was used as a constant value of 1.47×10^4, 3.48×10^3, and 8.62×10^2 kPa for SM, ML, and CL soils, respectively.
- Undrained shear strength (S_u) for ML in embankment: A constant value of 38.3 kPa (800 psf) was assigned to model the undrained strength of the ML layer under flood loading.

Boundary Conditions

The bottom boundary was constrained in both the vertical and horizontal directions. For the flow boundary conditions, the bottom boundary was set as impermeable. The total head was applied to the left boundary according to the specified elevation of the water as a function of time on the levee (hydrograph), no flow was applied to the right boundary of the embankment, and the total head equal to the ground elevation was applied on the landside or right boundary of the foundation.

Modeling Stages

The simulation for the historical and the projected flood levels consisted of two stages. It is noted that the landside and riverside ground elevations were different (as shown in Fig. 2). The first stage involved generation of a steady-state seepage flow throughout the levee domain as the initial hydraulic condition. In this stage, the simulation was started with an initial condition of total head defined at the elevation of the landside ground surface throughout the levee. Total hydraulic heads of 18.3 and 17.0 m were then assigned to the riverside and landside, which represent the ground surface elevation at the riverside and landside, respectively. Seepage analysis was performed to achieve a steady state condition under the assigned boundary conditions. In the second stage (transient stage), the water level behind the levee was raised at a constant rate of 6 cm/hour until reaching the peak flood level for each scenario (shown in Table 1). Then, the flood peak was maintained for several days until a steady-state condition was reached. The flood modeling stage is consistent with the approach commonly used by operational agencies (e.g., USACE 2000) and other similar studies. For example, Khalilzad et al. (2014) employed the same approach for modeling the Elkhorn Levee.

Results and Discussion

This section presents and discusses results of the probabilistic seepage-slope stability modeling for the three failure modes examined (underseepage at toe, uplift at toe, and slope stability for the landside slope) using historical and future flood scenarios. For each mode, the probability of failure at each time was determined as the fraction of 6,000 Monte Carlo realizations that failed to satisfy the performance criteria for that mode of failure. Further, for each mode and at each specified time, factors of safety corresponding to 6,000 realizations were averaged to estimate the mean factor of safety. Lower and upper bounds for the probability of failure considering combined mode of failure were also calculated and presented. The primary emphasis was on the comparison between the results of the historical floods versus those from future floods. The probabilities of failure that are presented are probabilities of failure for particular scenarios. The presented results represent changes in conditional probabilities of failure (i.e., conditioned on the given scenarios). These are different than the probability of failure at different return periods. For instance, the probabilities of failure shown in the following sections for a recurrence interval of 50 years are not the probabilities of failure over a 50-year period. The latter would have to account for the frequency at which these scenarios occur.

Underseepage

Fig. 4 shows the mean factor of safety against underseepage at toe versus time using the historical and future flood scenarios for three

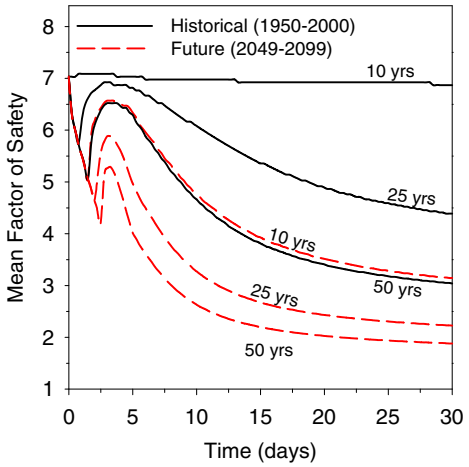

Fig. 4. Mean factor of safety for underseepage at the toe versus time using the historical and future 10-, 25-, and 50-year flood simulations.

recurrence intervals of 10, 25, and 50 years. For all recurrence intervals and climate scenarios, the mean factor of safety decreased as the water level approached the flood peak and continued to further decrease even after the water level was maintained at the peak flood, reaching an almost plateau toward the end of simulations.

These curves in Fig. 4 illustrate the buildup of excess pore-water pressure and release in soils with relatively low hydraulic conductivity. Higher water levels increase total head due to the higher hydraulic boundary conditions. In the coupled analysis, the forces were also considered from the increase of water load on the embankment. Because the soil particles and water were considered incompressible, this extra load was first seen by "excess" pore-water pressure (those that were above what would be realized by hydraulic boundary conditions only in an uncoupled computation). So, in the 50-year future curve, a strong decrease in the mean factor of safety was seen until around 2.5 days. Beyond this point, the mean factor of safety reached a plateau. When given a chance, the built-up excess pore-water pressure was dissipated, and that is what is shown in the results by the mean factor of safety going up as the total head went down during this process. However, because the water on the levee stayed constant at its highest level, the mean factor of safety started falling again and eventually reached a steady-state value.

The 50-year current hydrograph reached its maximum height at around 1.6 days, so the downturn in mean factor of safety for underseepage occurred at that time but did not get nearly as low as with the larger 50-year future simulated event. Therefore, we see that the stronger the rise of the water level for a given event, the more profound the coupled effect is. All results showed this dip and rebound, but this behavior was more pronounced in under-seepage results than uplift or slope stability results. This is because the exit gradient represents a type of derivative $(\Delta\phi/\Delta y)$ at the toe, whereas uplift and slope stability just involve parameter values. Derivatives can magnify changes. Finally, in an uncoupled analysis, parameter values do not experience this dip and rebound effect but simply increase monotonically, and with enough time will achieve steady state.

This explains why the mean factor of safety against underseepage for the future flood was much less than those for the historical flood in all recurrence intervals. In all cases, the mean factor of safety against underseepage was 7.03 in the beginning (initial steady-state condition). For the 50-year flood, the mean factor of safety decreased to 3.04 and 1.88 after 30 days by applying the historical and future floods, respectively. For the 10-year flood, applying the historical flood data led to a mean factor of safety of 6.87 against underseepage after 30 days, whereas a mean factor of safety of 3.15 was attained for the same case by imposing the future flood data.

A similar behavior was seen when studying this mode of failure (Fig. 5). The probability of failure against underseepage was almost zero in the initial steady-state condition. When using the historical flood simulations, the probability of failure due to underseepage was zero, 0.05, and 0.36 at the end of modeling for 10-, 25-, and 50-year floods, respectively. Employing the future floods significantly increased the probability of failure due to underseepage, resulting in 0.32, 0.71, and 0.84 probability of failure against underseepage for 10-, 25-, and 50-year floods, respectively. This observation signifies the importance of considering the climate change for levee risk analysis under flooding. It is also important to note the dip and rebound that occurred in these results, with the 50-year future being the most dramatic and occurring again at 2.5 days (when the hydrograph stopped increasing and the excess pore-water pressure began to dissipate).

Uplift

Fig. 6 depicts the mean factor of safety against uplift at the toe versus time for historical and future flood scenarios at different recurrence intervals. The factor of safety against uplift was 1.61 in the beginning and continuously decreased for all cases until reaching an almost steady state toward the end of simulations. Like the underseepage results, employing the future floods led to significantly lower factors of safety against uplift compared to the historical flood scenario. The mean factor of safety against uplift was 1.60, 1.46, and 1.32 after 30 days by applying 10-, 25-, and 50-year historical flood data, respectively. It is noted that the mean factor of safety for 10-year historical flood data remained almost unchanged, which is due to the fact that the flood level for this scenario (Table 1) raised only few centimeters above the riverside ground surface (Fig. 2). For the same cases but using the future floods, the mean factor of safety against uplift was found to be 1.33, 1.21, and 1.15 after 30 days for 10-, 25-, and 50-year flood data.

Fig. 7 illustrates the probability of failure against uplift for different historical and projected flooding. The trends are consistent with those in Fig. 6. The probability of failure against uplift was zero in the initial condition. With the historical flood data, the probability of failure due to uplift was zero, 0.73, and 0.95 at the end of simulations for 10-, 25-, and 50-year floods, respectively. These values increased to 0.94, 0.99, and 1.00 for 10-, 25-, and 50-year

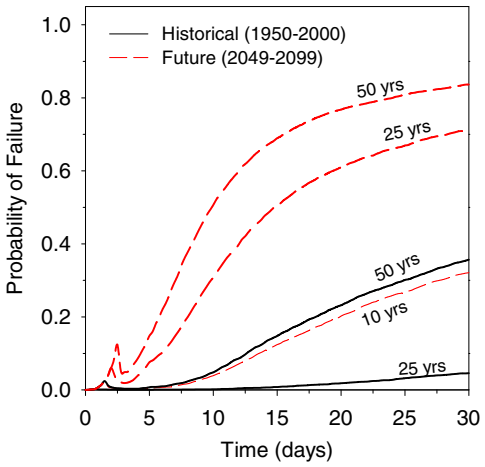

Fig. 5. Probability of failure for underseepage at the toe versus time using the historical and future 10-, 25-, and 50-year flood simulations.

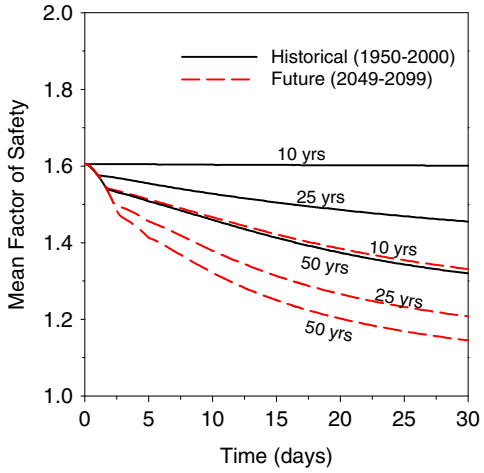

Fig. 6. Mean factor of safety for uplift at the toe versus time using the historical and future 10-, 25-, and 50-year flood simulations.

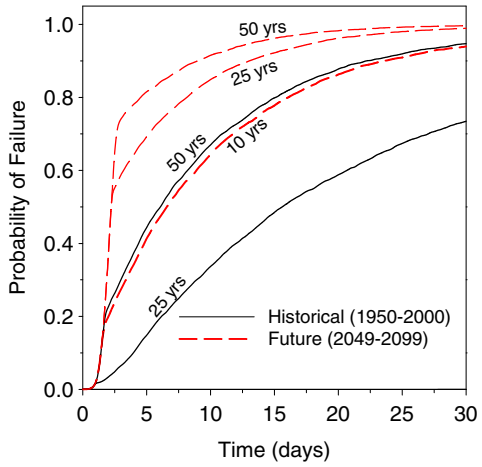

Fig. 7. Probability of failure for uplift at the toe versus time using the historical and future 10-, 25-, and 50-year flood simulations.

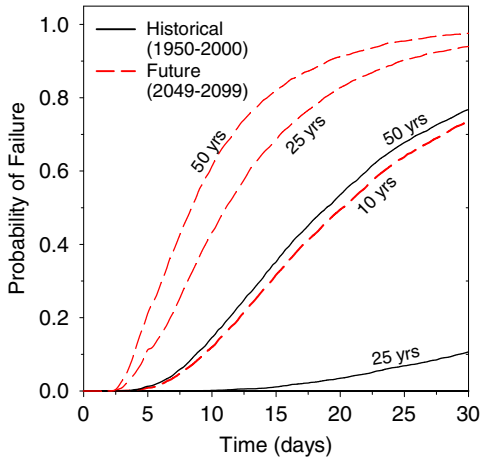

Fig. 9. Probability of failure for slope stability versus time using the historical and future 10-, 25-, and 50-year flood simulations.

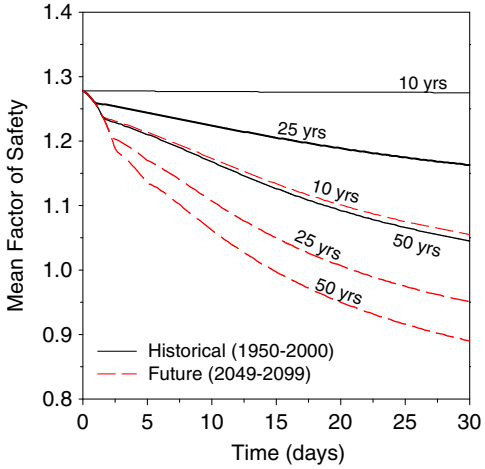

Fig. 8. Mean factor of safety for slope stability versus time using the historical and future 10-, 25-, and 50-year flood simulations.

floods, respectively, for the future flooding scenario. Overall, the levee showed very high probabilities of failure against uplift for almost all cases, except the 10-year historical flood. For the 10-year flooding, using the future data led to a drastic increase in the probability of failure (from zero to 0.94), which is due to the significant increase (2.13 m) in the flood level obtained for these two cases (Table 1).

Slope Stability

Fig. 8 provides a comparison between the mean factors of safety for slope stability of the landside slope versus time for different recurrence intervals using historical versus future floods. The mean factor of safety was 1.28 initially, and then decreased with time. Under the historical flooding scenario, it reached to 1.28, 1.16, and 1.05 after 30 days for 10-, 25-, and 50-year floods. For the same cases but using the future flood data, the mean factor of safety dropped to 1.06, 0.95, and 0.89 for 10-, 25-, and 50-year floods, respectively. The landside slope initially exhibited a marginal stability, which was further degraded by the introduction of the flood, bringing the mean factor of safety even below the limit state. Longer duration and higher flood levels increased the pore-water pressure within the level embankment, which led to a reduction in the soil's shear strength, degrading the stability of the levee. Incorporating the future climate (i.e., higher flood stage) rather than relying on the historical dataset resulted in a further decrease in the factor of safety against slope stability.

Fig. 9 shows the probability of failure for slope stability. Consistent with the tendancies discussed for Fig. 8, the probability of failure increased with time and reached very high values in most cases (e.g., 0.94 and 0.98 for the 25- and 50-year future floods). The probability of failure for the 10-year historical flood exhibited an almost constant value over time, because the water level did not increase considerably with time for this case. When the projected future flood was applied, the probability of failure was significantly higher compared to those attained using the historical floods.

Combined Mode of Failure

Fig. 10 shows the probability of failure in combined failure modes for various flood water levels using historical and future flood events considering different recurrence intervals. The upper and lower bounds for the combined probability of failure were determined by employing the individual probabilities of failure along with Eq. (6). The combined probability of failure provides an effective measure to properly assess overall levee performance. For all cases, the results from the lower and upper bounds were close, leading to a narrow band. Considering the combined mode of failure, the probability of failure quickly approached to one for 25- and 50-year future floods. Also, the probability of failure significantly increased toward higher recurrence intervals with high water level.

Relative Changes in Results for Past versus Future Flood Scenarios

Table 3 summarizes the relative decreases in the mean factor of safety and the relative increases in the probability of failure for different modes of failure and recurrence intervals using the future compared to the historical flood data. In each case, the relative change percentage was calculated as (future-historical)/historical. The future floods significantly decrease the mean factor of safety and increase the probability of failure for all modes and recurrence intervals. The highest relative reduction in the mean factor of safety was found to be 54.2% for underseepage for the 10-year flood scenario. Among different modes of failure, underseepage had the

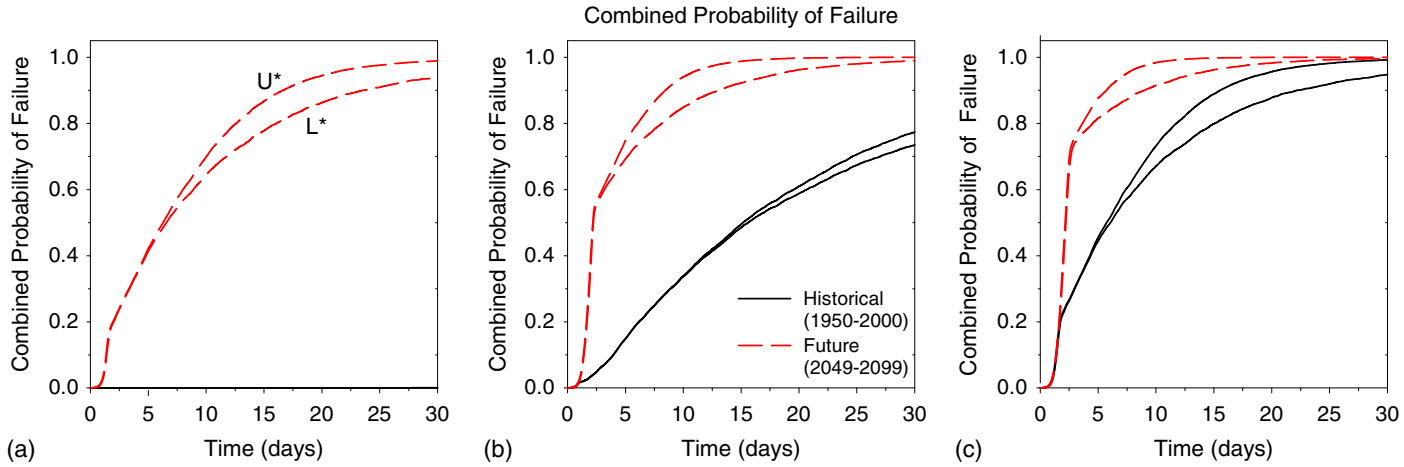

Fig. 10. Upper and lower bounds for combined probability of failure versus time using the historical and future flood scenarios for different recurrence intervals: (a) 10 years; (b) 25 years; and (c) 50 years.

Table 3. Relative decrease in mean factor of safety and relative increase in probability of failure for different modes of failure and recurrence intervals using future compared to historical flood data

Performance metric	Recurrence interval (years)	Relative change in results using future versus past floods				
		Underseepage	Uplift	Slope stability	Combined—lower bound	Combined—upper bound
Decrease in mean factor of safety (%)	10	54.2	16.9	17.3	—	—
	25	49.3	17.0	18.2	—	—
	50	38.1	13.3	14.8	—	—
Increase in probability of failure (%)	10	≫100	≫100	≫100	≫100	≫100
	25	100	34.6	≫100	34.6	29.2
	50	100	5.2	27.1	5.2	0.8

largest change for the future flood scenarios. Further, the impact of using future flooding is more pronounced for shorter recurrence intervals (e.g., 10-year). This can be from the significant increase in projected future flood levels for 10-year events (shown in Table 1). For the 10-year events, because the historical probabilities of failure were very low, the dominator in the relative difference was very small, exaggerating relative differences. For these cases, a relative difference of ≫100% was reported in Table 3. For the 25- and 50-year events, the probability of failure increased as much as 100% for the cases examined.

This study presented a systematic framework for translating large-scale climate information down to local-scale engineering applications, an aspect that has been indemnified as a critical gap in the state of the art and practice by the Fourth National Climate Assessment model (Reidmiller et al. 2017). This framework allows engineers and other stakeholders to perform levee risk analysis while accounting for possible effects of climate change. While the impact can be significant in one region/levee system, it might be insignificant in another area/levee system. The approach introduced in this study can be applied to a wide array of levee systems to quantify the impact of climate change on the integrity and reliability of levees.

Conclusions

The warming climate and its consequences cause changes in severity, frequency, and duration of extreme precipitation and flooding, which can significantly affect the integrity and performance of levees. This study incorporated a set of historical and projected flood levels into a fully coupled finite-element seepage –limit equilibrium slope stability model to numerically evaluate the fragility of the Elkhorn Levee in Sacramento, California, against multiple modes of failures including slope stability, underseepage, and uplift. The projected design floods were obtained using a nonstationary framework and climate model simulations. The results obtained from historical (baseline) and future flood simulations are evaluated against each other to quantify climate change impact on the levee integrity.

The results showed that future flood events could significantly increase the levee's probability of failure against individual and combined modes of underseepage, uplift and slope stability. For all cases, an increase in the flood level of all recurrence intervals significantly impacts the overall stability in the future relative to the past. For the cases examined, the results showed up to 54% reduction in safety factor and over 100% increase in the probability of failure when considering the future versus historical flood scenarios. Any changes in the statistics of extreme events due to climate change will directly impact the overall stability of levees. The proposed framework in this study can be adopted as a basis for performing risk analysis of geotechnical structures under changes in climatic extreme events. Integrating concepts from geotechnical engineering, hydrology, and climate science, this study demonstrated how a multidisciplinary approach can be employed to quantify site-specific impacts of climate change on earthen infrastructure [i.e., translating large-scale climate information down to local-scale applications—this is identified as one of the current gaps in the Fourth National Climate Assessment model (USGCRP 2018)]. The probabilistic methodology presented in this study requires very

limited in situ data (such as geometry and soil type) and can be broadly applicable to the nation's portfolio of levees while accounting for the uncertainly of soil parameters.

The focus in this paper was presenting a methodological framework to integrate climate model simulations for analyzing the integrity of infrastructure systems. For site-specific engineering applications, depending on the location and driving forces, different types of inputs and design variables may be required. Further, to account for intermodel variability and uncertainty in model simulations and future scenarios, we recommend using multiple climate model simulations and representative concentration pathways. The approach would be very similar to this study but would involve running more simulations using different climate models and/or future scenarios. Given that our goal here was to introduce a methodological framework, we did not use a wide range of scenarios, so we cannot claim that this is a comprehensive local-scale future flood risk analysis.

Data Availability Statement

Some or all data, models, or code generated or used during the study are available from the corresponding author by request. These data and models include the model for finite-element simulations and the code used for ProNEVA.

Acknowledgments

This material is based upon work supported in part by the National Science Foundation under Grant Nos. CMMI-1634748 and CMMI-1635797. This work was also supported in part by a grant of computer time from the Department of Defense (DoD) High Performance Computing Modernization Program (HPCMP), with computer time granted on the ERDC DoD Supercomputing Center (DSRC) Cray XC40 system named "Onyx." We acknowledge the World Climate Research Programme's Working Group on Coupled Modeling, which is responsible for CMIP, and we thank the climate-modeling groups for producing and making available their model output. For CMIP, the DOE's Program for Climate Model Diagnosis and Intercomparison (PCMDI) provides coordinating support and leads the development of software infrastructure in partnership with the Global Organization for Earth System Science Portals. We also thank Daniel Cayan, David Pierce, and Julie Kalansky from Scripps Institution of Oceanography, University of California, San Diego, for providing downscaled and routed streamflow and gridded runoff projections over California. The bias-corrected model simulations for the state of California are available from the Cal-Adapt (https://cal-adapt.org/). The authors would like to thank Dr. Ghada Ellithy for her assistance during the revision of this paper. Constructive review comments and suggestions from an anonymous associate editor and three reviewers are greatly appreciated.

References

ASCE. 2017. *2017 infrastructure report card*. Reston, VA: ASCE. www.infrastructurereportcard.org.

Baecher, G. B., and J. T. Christian. 2003. *Reliability and statistics in geotechnical engineering*. Chichester, UK: Wiley.

Bessette, D. L., L. A. Mayer, B. Cwik, M. Vezer, K. Keller, R. J. Lempert, and N. Tuana. 2017. "Building a values-informed mental model for New Orleans climate risk management." *Risk Anal.* 37 (10): 1993–2004. https://doi.org/10.1111/risa.12743.

Bogárdi, I., and E. Balogh. 2014. "Floodway system operation along levee-protected rivers." *J. Water Resour. Plann. Manage.* 140 (8): 04014014. https://doi.org/10.1061/(ASCE)WR.1943-5452.0000391.

Brizendine, A. L. 1997. "Risk based analysis of levees." Ph.D. dissertation, College of Engineering and Mineral Resources, West Virginia Univ.

Brooks, B. A., G. Bawden, D. Manjunath, C. Werner, N. Knowles, J. Foster, J. Dudas, and D. R. Cayan. 2012. "Contemporaneous subsidence and levee overtopping potential, Sacramento-San Joaquin Delta, California." *San Francisco Estuary Watershed Sci.* 10 (1). https://doi.org/10.15447/sfews.2012v10iss1art4.

CACC (Committee on Adaptation to a Changing Climate). 2018. *Climate resilient infrastructure: A manual of practice on adaptive design and risk management*. Reston, VA: ASCE.

CDWR (California Department of Water Resources). 2011. *Flood control system status report*. Sacramento, CA: CDWR.

Chen, X., and F. Hossain. 2019. "Understanding future safety of dams in a changing climate." *Bull. Am. Meteorol. Soc.* 100 (8): 1395–1404. https://doi.org/10.1175/BAMS-D-17-0150.1.

Cheng, L., A. AghaKouchak, E. Gilleland, and R. W. Katz. 2014. "Non-stationary extreme value analysis in a changing climate." *Clim. Change* 127 (2): 353–369. https://doi.org/10.1007/s10584-014-1254-5.

Deverel, S. J., S. Bachand, S. J. Brandenberg, C. E. Jones, J. P. Stewart, and P. Zimmaro. 2016. "Factors and processes affecting delta levee system vulnerability." *San Francisco Estuary Watershed Sci.* 14 (4). https://doi.org/10.15447/sfews.2016v14iss4art3.

Deverel, S. J., and D. A. Leighton. 2010. "Historic, recent, and future subsidence, Sacramento-San Joaquin Delta, California, USA." *San Francisco Estuary Watershed Sci.* 8 (2). https://doi.org/10.15447/sfews.2010v8iss2art1.

England, J. F., Jr., T. A. Cohn, B. A. Faber, J. R. Stedinger, W. O. Thomas Jr., A. G. Veilleux, J. E. Kiang, and R. R. Mason Jr. 2019. *Guidelines for determining flood flow frequency—Bulletin 17C*. Rep. No. 4-B5. Reston, VA: USGS.

FEMA. 2018. *2018 national preparedness report*. Washington, DC: FEMA. https://www.fema.gov/media-library/assets/documents/170861.

Fletcher, S., M. Lickley, and K. Strzepek. 2019. "Learning about climate change uncertainty enables flexible water infrastructure planning." *Nat. Commun.* 10 (1): 1–11. https://doi.org/10.1038/s41467-019-09677-x.

Florsheim, J. L., and M. D. Dettinger. 2007. "Climate and floods still govern California levee breaks." *Geophys. Res. Lett.* 34 (22): L22403. https://doi.org/10.1029/2007GL031702.

Florsheim, J. L., and J. F. Mount. 2003. "Changes in lowland floodplain sedimentation processes: Pre-disturbance to post-rehabilitation, Cosumnes River, California." *Geomorphology* 56 (3–4): 305–323. https://doi.org/10.1016/S0169-555X(03)00158-2.

Forzieri, G., A. Bianchi, F. B. e Silva, M. A. M. Herrera, A. Leblois, C. Lavalle, J. C. Aerts, and L. Feyen. 2018. "Escalating impacts of climate extremes on critical infrastructures in Europe." *Global Environ. Change* 48 (Jan): 97–107. https://doi.org/10.1016/j.gloenvcha.2017.11.007.

Fredlund, D., A. Xing, and S. Huang. 1994. "Predicting the permeability function for unsaturated soils using the soil-water characteristic curve." *Can. Geotech. J.* 31 (4): 533–546. https://doi.org/10.1139/t94-062.

Fredlund, D. G., and A. Xing. 1994. "Equations for the soil-water characteristic curve." *Can. Geotech. J.* 31 (4): 521–532. https://doi.org/10.1139/t94-061.

Groisman, P. Y., R. W. Knight, T. R. Karl, D. R. Easterling, B. Sun, and J. H. Lawrimore. 2004. "Contemporary changes of the hydrological cycle over the contiguous United States: Trends derived from in situ observations." *J. Hydrometeorol.* 5 (1): 64–85. https://doi.org/10.1175/1525-7541(2004)005<0064:CCOTHC>2.0.CO;2.

Groves, R. M. 2006. "Nonresponse rates and nonresponse bias in household surveys." *Public Opin. Q.* 70 (5): 646–675. https://doi.org/10.1093/poq/nfl033.

Hagenlocher, M., F. G. Renaud, S. Haas, and Z. Sebesvari. 2018. "Vulnerability and risk of deltaic social-ecological systems exposed to multiple hazards." *Sci. Total Environ.* 631–632 (Aug): 71–80. https://doi.org/10.1016/j.scitotenv.2018.03.013.

Holtz, R. D., W. D. Kovacs, and T. C. Sheahan. 2011. *An introduction to geotechnical engineering*. 2nd ed. London: Pearson.

Hui, R., J. Herman, J. Lund, and K. Madani. 2018. "Adaptive water infrastructure planning for nonstationary hydrology." *Adv. Water Resour.* 118 (Aug): 83–94. https://doi.org/10.1016/j.advwatres.2018.05.009.

Hui, R., E. Jachens, and J. Lund. 2016. "Risk-based planning analysis for a single levee." *Water Resour. Res.* 52 (4): 2513–2528. https://doi.org/10.1002/2014WR016478.

IPCC (Intergovernmental Panel on Climate Change). 2013. *Climate change 2013: The physical science basis*. Contribution of Working Group I to the Fifth Assessment Report of the Intergovernmental Panel on Climate Change Cambridge University Press. Cambridge, UK: IPCC.

Jasim, F. H., F. Vahedifard, E. Ragno, A. AghaKouchak, and G. Ellithy. 2017. "Effects of climate change on fragility curves of earthen levees subjected to extreme precipitations." In *Geo-Risk 2017: Geotechnical Risk Assessment and Management*, Geotechnical Special Publication 285, edited by J. Huang, G. A. Fenton, L. Zhang, and D. V. Griffiths, 498–507. Reston, VA: ASCE.

Jongejan, R., B. Maaskant, W. ter Horst, F. Havinga, N. Roode, and H. Stefess. 2013. "The VNK2-project: A fully probabilistic risk analysis for all major levee systems in the Netherlands." In Vol. 357 of *Proc., Floods: From Risk to Opportunity*, 75–85. Oxfordshire, UK: International Association of Hydrological Sciences.

Jongejan, R. B., and E. O. F. Calle. 2013. "Calibrating semi-probabilistic safety assessments rules for flood defenses." *Georisk: Assess. Manage. Risk Eng. Syst. Geohazards* 7 (2): 88–98. https://doi.org/10.1080/17499518.2013.790731.

Khalilzad, M., M. A. Gabr, and M. E. Hynes. 2014. "Effects of woody vegetation on seepage-induced deformation and related limit state analysis of levees." *Int. J. Geomech.* 14 (2): 302–312. https://doi.org/10.1061/(ASCE)GM.1943-5622.0000304.

Kundzewicz, Z. W., et al. 2014. "Flood risk and climate change: Global and regional perspectives." *Hydrol. Sci. J.* 59 (1): 1–28. https://doi.org/10.1080/02626667.2013.857411.

Lanzafame, R., and N. Sitar. 2019. "Reliability analysis of the influence of seepage on levee stability." *Environ. Geotech.* 6 (5): 284–293. https://doi.org/10.1680/jenge.18.00060.

LAO (Legislative Analyst's Office). 2015. *Achieving state goals for the Sacramento-San Joaquin Delta*. Sacramento, CA: LAO.

Lendering, K., T. Schweckendiek, and M. Kok. 2018. "Quantifying the failure probability of a canal levee." *Georisk: Assess. Manage. Risk Eng. Syst. Geohazards* 12 (3): 203–217. https://doi.org/10.1080/17499518.2018.1426865.

Lohmann, D., E. Raschke, B. Nijssen, and D. P. Lettenmaier. 1998. "Regional scale hydrology. II: Application of the VIC-2L model to the Weser River, Germany." *Hydrol. Sci. J.* 43 (1): 143–158. https://doi.org/10.1080/02626669809492108.

Lohmann, D. A. G., R. Nolte-Holube, and E. Raschke. 1996. "A large-scale horizontal routing model to be coupled to land surface parametrization schemes." *Tellus A* 48 (5): 708–721. https://doi.org/10.3402/tellusa.v48i5.12200.

Ludy, J., and G. Kondolf. 2012. "Flood risk perception in lands protected by 100-year levees." *Nat. Hazards* 61 (2): 829–842. https://doi.org/10.1007/s11069-011-0072-6.

Mallakpour, I., M. Sadegh, and A. AghaKouchak. 2018. A new normal for streamflow in California in a warming climate: Wetter wet seasons and drier dry seasons." *J. Hydrol.* 567: 203–211.

Mayne, P. W. 2012. "Quandary in geomaterial characterization: New versus the old." In *Shaking the foundations of geo-engineering education*, edited by B. McCabe, M. Pantazidou, and D. Phillips. Boca Raton, FL: CRC Press.

NLD (National Levee Database). 2020. "National levee database, segment name: RD 1000-Natomas." Accessed February 15, 2020. https://levees.sec.usace.army.mil/#/map-viewer/search/sy=@name:natomas.

Papalexiou, S. M., and A. Montanari. 2019. "Global and regional increase of precipitation extremes under global warming." *Water Resour. Res.* 55 (6): 4901–4914. https://doi.org/10.1029/2018WR024067.

Pielke, R. A., M. W. Downton, and J. B. Miller. 2002. *Flood damage in the United States, 1926–2000: A reanalysis of national weather service estimates*. Boulder, CO: Univ. Corporation for Atmospheric Research.

Pierce, D. W., D. R. Cayan, E. P. Maurer, J. T. Abatzoglou, and K. C. Hegewisch. 2015. "Improved bias correction techniques for hydrological simulations of climate change." *J. Hydrometeorol.* 16 (6): 2421–2442. https://doi.org/10.1175/JHM-D-14-0236.1.

Pierce, D. W., D. R. Cayan, and B. L. Thrasher. 2014. "Statistical downscaling using localized constructed analogs (LOCA)." *J. Hydrometeorol.* 15 (6): 2558–2585. https://doi.org/10.1175/JHM-D-14-0082.1.

Pierce, D. W., J. F. Kalansky, and D. R. Cayan. 2018. *Climate, drought, and sea level rise scenarios for the fourth California climate assessment*. California's Fourth Climate Change Assessment. Publication No. CNRA-CEC-2018-006. San Diego, CA: California Energy Commission, Scripps Institution of Oceanography.

Ragno, E., A. AghaKouchak, C. A. Love, L. Cheng, F. Vahedifard, and C. H. R. Lima. 2019. "Quantifying changes in future intensity-duration-frequency curves using multi-model ensemble simulations." *Water Resour. Res.* 54 (3): 1751–1764. https://doi.org/10.1002/2017WR021975.

Rahimi, M., N. L. Dehghani, and A. Shafieezadeh. 2019. "Probabilistic lifecycle cost analysis of levees against backward erosion." In *Proc., Int. Conf. on Sustainable Infrastructure 2019: Leading Resilient Communities through the 21st Century*, 566–574. Reston, VA: ASCE.

Reidmiller, D. R., C. W. Avery, D. R. Easterling, K. E. Kunkel, K. L. Lewis, T. K. Maycock, and B. C. Stewart. 2017. Vol. 2 of *Impacts, risks, and adaptation in the United States: Fourth national climate assessment*. Washington, DC: US Global Change Research Program.

Rice, J. D., and L. Polanco. 2012. "Reliability-based underseepage analysis in levees using a response surface–Monte Carlo simulation method." *J. Geotech. Geoenviron. Eng.* 138 (7): 821–830. https://doi.org/10.1061/(ASCE)GT.1943-5606.0000650.

Robinson, J. D., and F. Vahedifard. 2016. "Weakening mechanisms imposed on California's levees under multiyear extreme drought." *Clim. Change* 137 (1–2): 1–14. https://doi.org/10.1007/s10584-016-1649-6.

Robinson, J. D., F. Vahedifard, and A. AghaKouchak. 2017. "Rainfall-triggered slope instabilities under a changing climate: Comparative study using historical and projected precipitation extremes." *Can. Geotech. J.* 54 (1): 117–127. https://doi.org/10.1139/cgj-2015-0602.

Roe, E., R. G. Bea, S. N. Jonkman, H. Faucher De Corn, H. Foster, J. Radke, P. Schulman, and R. Storesund. 2016. "Risk assessment and management for interconnected critical infrastructure systems at the site and regional levels in California's Sacramento-San Joaquin Delta." *Int. J. Crit. Infrastruct.* 12 (1–2): 143–174. https://doi.org/10.1504/IJCIS.2016.075867.

Salas, J. D., and J. Obeysekera. 2014. "Revisiting the concepts of return period and risk for nonstationary hydrologic extreme events." *J. Hydrol. Eng.* 19 (3): 554–568. https://doi.org/10.1061/(ASCE)HE.1943-5584.0000820.

Schultz, M. T., B. P. Gouldby, J. D. Simm, and J. L. Wibowo. 2010. *Beyond the factor of safety: Developing fragility curves to characterize system reliability.* Rep. No. ERDC-SR-10-1. Vicksburg, MS: Engineer Research and Development Center, Geotechnical and Structures Laboratory.

Schultz, M. T., F. T. Tracy, G. S. Ellithy, D. W. Harrelson, J. L. Ryder, and M. K. Corcoran. 2018. "Characterizing the reliability of earthen levees using system response curves derived from uncertainty analysis of geotechnical simulation models." In *Proc., 38th Annual Conf. & Exhibition of the United States Society on Dams (USSD)*. Westminster, CO: United States Society on Dams. http://ussd2019.conferencespot.org/65175-ussd-1.4163582/t001-1.4164397/2f-1.4164424/a051-1.4164437/an051-1.4164438#tab%200=1.

Thorne, J. H., H. Choe, P. A. Stine, J. C. Chambers, A. Holguin, A. C. Kerr, and M. W. Schwartz. 2018. "Climate change vulnerability assessment of forests in the Southwest USA." *Clim. Change* 148 (3): 387–402.

Tracy, F. T., J. L. Ryder, M. T. Schultz, G. S. Ellithy, B. R. Breland, T. C. Massey, and M. K. Corcoran. 2020. "Monte Carlo simulations of coupled transient seepage flow and soil deformation in levees." *Scalable Comput.: Pract. Experience* 21 (1): 147–156. https://doi.org/10.12694/scpe.v21i1.1629.

Trenberth, K. E. 2001. "Stronger evidence of human influences on climate: The 2001 IPCC Assessment." *Environ: Sci. Policy Sustainable Dev.* 43 (4): 8–19. https://doi.org/10.1080/00139150109605136.

USACE. 1999. *Evaluating the reliability of existing levees*. Appendix B, Engineering Technical Letter ETL 1110-2-556. Washington DC: USACE.

USACE. 2000. *Design and construction of levees*. Engineer Manual No. EM 1110-2-1913. Washington DC: USACE.

USBR (United States Bureau of Reclamation). 2019. "Best practices in dam and levee safety risk analysis." Accessed July 1, 2019. https://www.usbr.gov/ssle/damsafety/risk/BestPractices/Chapters/1-BestPracticesCover.pdf.

USGCRP (US Global Change Research Program). 2009. *Global climate change impacts in the United States*. Washington, DC: Cambridge University Press.

USGCRP (US Global Change Research Program). 2018. "Fourth national climate assessment." Accessed October 8, 2019. https://nca2018.globalchange.gov.

Vahedifard, F., A. AghaKouchak, and J. D. Robinson. 2015. "Drought threatens California's levees." *Science* 349 (6250): 799. https://doi.org/10.1126/science.349.6250.799-a.

Vahedifard, F., J. D. Robinson, and A. AghaKouchak. 2016. "Can protracted drought undermine the structural integrity of California's earthen levees?" *J. Geotech. Geoenviron. Eng.* 142 (6): 02516001. https://doi.org/10.1061/(ASCE)GT.1943-5606.0001465.

Vahedifard, F., F. S. Tehrani, V. Galavi, E. Ragno, and A. AghaKouchak. 2017. "Resilience of MSE walls with marginal backfill under a changing climate: Quantitative assessment for extreme precipitation events." *J. Geotech. Geoenviron. Eng.* 143 (9): 04017056. https://doi.org/10.1061/(ASCE)GT.1943-5606.0001743.

Vahedifard, F., J. M. Williams, and A. AghaKouchak. 2018. "Geotechnical engineering in the face of climate change: Role of multi-physics processes in partially saturated soils." In *IFCEE 2018: Advances in Geomaterial Modeling and Site Characterization*, Geotechnical Special Publication 295, edited by A. W. Stuedlein, A. Lemnitzer, and M. T. Suleiman, 353–364. Reston, VA: ASCE.

Vardon, P. J. 2015. "Climatic influence on geotechnical infrastructure: A review." *Environ. Geotech.* 2 (3): 166–174. https://doi.org/10.1680/envgeo.13.00055.

White, E. L. 1976. "Role of carbonate rocks in modifying extreme flow behavior." *J. Am. Water Resour. Assoc.* 12: 351–370. https://doi.org/10.1111/j.1752-1688.1976.tb02684.x.

Witczak, M. W., W. N. Houston, C. E. Zapata, C. Richter, G. Larson, and K. Walsh. 2000. *Guide for mechanistic-empirical design of new and rehabilitated pavement structures. Appendix DD-4: Improvement of the integrated climatic model for moisture content predictions*. Final Rep. to National Cooperative Highway Research Program. Rep. No. 1-37A. Washington, DC: Transportation Research Board.

Wobus, C., M. Lawson, R. Jones, J. Smith, and J. Martinich. 2014. "Estimating monetary damages from flooding in the United States under a changing climate." *J. Flood Risk Manage.* 7 (3): 217–229. https://doi.org/10.1111/jfr3.12043.

Wolff, T. F. 2008. "Reliability of levee systems." In *Reliability-based design in geotechnical engineering: Computations and applications*, edited by K.-K. Phoon, 530. New York: Routledge.

Wood, E. 1977. "An analysis of flood levee reliability." *Water Resour. Res.* 13 (3): 665–671. https://doi.org/10.1029/WR013i003p00665.

Wu, S. J., J. C. Yang, and Y. K. Tung. 2011. "Risk analysis for flood control structure under consideration of uncertainties in design flood." *Nat. Hazards* 58 (1): 117–140. https://doi.org/10.1007/s11069-010-9653-z.

Zhang, L. M., Y. Xu, Y. Liu, and M. Peng. 2013. "Assessment of flood risks in Pearl River Delta due to levee breaching." *Georisk: Assess. Manage. Risk Eng. Syst. Geohazards* 7 (2): 122–133. https://doi.org/10.1080/17499518.2013.790733.

Zimmaro, P., J. P. Stewart, S. J. Brandenberg, D. Y. Kwak, and R. Jongejan. 2019. "Multi-hazard system reliability of flood control levees." *Soil Dyn. Earthquake Eng.* 124 (Sep): 345–353.